CZECH TECHNICAL UNIVERSITY IN PRAGUE

Faculty of Nuclear Sciences and Physical Engineering

Department of Physics

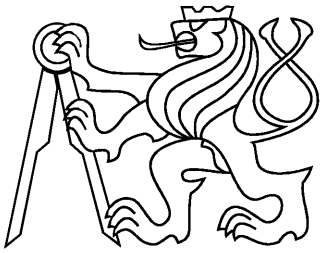

Research Work

Analysis of D^0 meson production in STAR experiment

Bc. Jana Crkovská

Supervisor: Mgr. Jaroslav Bielčík, Ph.D.

Consultant: Ing David Tlustý

Praha, 2013

Prohlášení:

Prohlašuji, že jsem svou bakalářskou práci vypracovala samostatně a použila jsem pouze podklady (literaturu, software, atd.) uvedené v přiloženém seznamu.

Nemám závažný důvod proti užití tohoto školního díla ve smyslu 60 Zákona .121/2000 Sb., o právu autorském, o právech souvisejících s právem autorským a o změně některých zákonů (autorský zákon).

V Praze dne 18. září 2013

Jana Crkovská

Title:
Analysis of D^0 meson production in STAR experiment

Author: Jana Crkovská

Specialization: Experimental nuclear and particle physics

Sort of project: Research work

Supervisor: Mgr. Jaroslav Bielčík, Ph.D.
Consultant: Ing. David Tlustý

Abstract:
The primary goal of the physics programme of the relativistic heavy-ion collisions investigations is to study the quark-gluon plasma (QGP). QGP is a very short-life state of matter and is therefore impossible to be detected directly. One of the possible probes for study of QGP are heavy-flavoured quarks. Measurement of charmonia and open-charm production can yield valuable information about the properties of QGP formed in the aftermath of the collision. This work deals with analysis of production of open-charm meson D^0 in U+U collisions at $\sqrt{s_{NN}} = 193$ GeV at STAR. The meson was reconstructed from its hadronic channel $D^0 \longrightarrow K^- + \pi^+$, which is easy to trigger and identify in the experiment.

Key words: relativistic heavy-ion collisions, STAR, heavy quarks, open-charm, quark-gluon plasma

Název práce:
Analýza produkce mezonu D^0 v experimentu STAR

Autor: Jana Crkovská

Abstrakt:

Primární cílem fyzikálního programu relativistických srážek těžkých iontů je studium kvark-gluononvého plazmatu (QGP). QGP je velmi krátce žijícím stavem hmoty a je proto nemožné jej detekovat přímo. Jednou z možných sond vhodných pro studium QGP jsou těžké kvarky. Z měření produkce charmonií či open-charm mezonů lze získat cenné informace o vlastnostech plazmatu vzniklého krátce po srážce. Tato práce shrnuje dosavadní výsledky analýzy produkce D^0 mezonu ve srážkách U+U při energii $\sqrt{s_{NN}} = 193$ GeV v experimentu STAR. Mezon byl rekonstruován z hadronového rozpadového kanálu $D^0 \longrightarrow K^- + \pi^+$, jehož produkty lze v experimentu STAR snadno identifikovat.

Klíčová slova: relativistické srážky těžkých iontů, STAR, těžké kvarky, open-charm, kvark-gluononvé plazma

Acknowledgement

I would like to express my gratitude to my supervisor Mgr. Jaroslav Bielčík, Ph.D. for his invaluable advice and support during this work. I would also like to thank to Ing. David Tlustý for his help with offline analysis and useful hints. I would also like to thank to my family for supporting me all that time.

Preface

Relativistic heavy-ion collisions provide a unique tool to study nuclear matter at extreme conditions. Similarly extreme conditions existed in the Early Universe, shortly after the Big Bang. A new state of matter – the quark-gluon plasma (QGP) – is predicted to be recreated in such high energy densities and temperatures. The QGP is a phase of deconfined quarks and gluons that behave asymptotically freely. The higher the temperature, the more does the medium properties resemble the primordial Universe. The first observation of QGP was recorded at Relativistic Heavy-Ion Collider (RHIC) at the Brookhaven National Laboratory.

QGP is created immediately after the collision – about $\tau \sim 1$ fs after the impact, the system is thermalised and in the state of perfect fluid. Yet shortly after (in order of few fs), the system reaches the freeze-out conditions. The QGP ceases to exist and the quarks and gluons reform into various hadrons. Sine it is so short-lived, the plasma cannot be observed directly. Several possible signatures were suggested: e. g. jet quenching, collective flow or suppression of heavy-flavoured hadrons.

The heavy quarks (charm c and beauty b) are a great probe of properties of the created system. Large amount of energy is necessary for their creation. Heavy quarks can be created during the initial phases of heavy-ion collision, when enough energy is released to the system. Modification of their properties can yield information about the hot and dense matter. Heavy quarks are predicted to behave differently to light quarks due to their large masses. In studies of heavy-hadrons production, quarkonia (bound systems of quark and antiquark of the same flavour) are of great importance. Spectral studies of heavy quarkonia can provide information of the medium temperature. The more excited states are easier to break and lower temperatures are necessary in order to achieve so. The measurement of production of open-charm and open-bottom hadrons serve as an independent complementary study to measurement of production of heavy quarkonia.

The heavy-ion collisions together with QGP and its signatures are discussed in Chapter 1. Then in Chapter 2, the previous D^0 measurement by STAR are mentioned. The STAR experiment and RHIC are briefly described in Chapter 3. In the final Chapter 4, the first results from the study of D^0 meson in U+U collisions at $\sqrt{s_{NN}} = 193$ GeV at STAR are presented. The D^0 meson was reconstructed from its hadronic decay $D^0 \longrightarrow K^- + \pi^+$.

Contents

List of Figures

List of Tables

Chapter 1

Introduction to relativistic heavy-ion collisions

1.1 Relativistic heavy-ion collisions

Collisions of ultra-relativistic nuclei serve as a unique tool to reproduce in laboratory the extreme conditions that prevailed in the early Universe shortly after the Big Bang. During this stage of very high energy densities and of high temperature,the matter is expected to exist in a state of Quark-Gluon Plasma (QGP). In the QGP, quarks and gluons are not confined in hadrons, but coexist freely in the hot and dense medium. This can be studied at the Relastivistic Heavy-Ion Collider (RHIC) at $\sqrt{s_{NN}} = 200$ GeV in Au+Au collisions and at the Large Hadron Collider (LHC) at $\sqrt{s_{NN}} = 2.75$ TeV in Pb+Pb collisions.

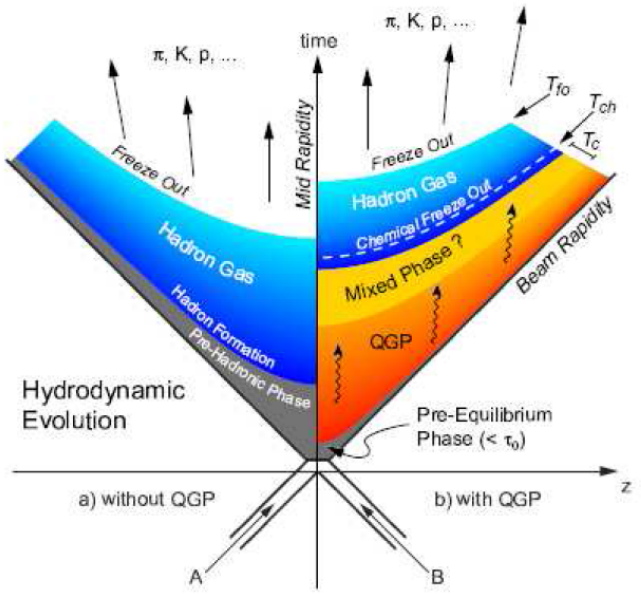

Figure 1.1: Space-time evolution of the heavy-ion collision without and with formation of QGP. Taken from [1].

A schematic diagram of the evolution of a relativistic heavy-ion collision is shown in Fig. 1.1 [1]. The QGP at RHIC is expected to last for about 10 fm/c. At about $\tau_0 \approx 1$ fm/c after the collision, the QGP is formed and the system starts to expand and cool down, until it reaches a critical temperature T_c. At that point the matter experiences a phase transition. The QGP stars to change into a hadron gas. At the point of chemical freeze-out, characterised by T_{ch}, the system is already fully in the state of a hadron gas. Multiplicities of single particle species are fixed at that time. The medium proceeds to cool and expand until the kinematical freeze-out T_{fo}. At T_{fo}, particles stop to interact and exchange the kinetic energy.

Due to the very short lifetime of the QGP phase, it cannot be observed directly. Only the hadrons in the final state can be measured.

1.2 Some signatures of the Quark-Gluon Plasma

Several observables are considered as signatures of the QGP. In the following text, we will discus some of them, namely suppresion of heavy-quark hadron production, jet quenching and flow [2, 3, 4, 5].

1.2.1 Suppresion of nuclear modification factor R_{AA}

Heavy quarks are produced in the early stages of the collision, during the initial hard scattering processes. They interact with the medium and the modification of their properties can therefore unveil new information about the medium.

To show how much the production of various particles is affected by the medium, the nuclear modification factor R_{AA} is used. R_{AA} is defined as a ratio of particle yield in A+A collision to the yield in p+p collision normalised by $\langle N_{bin} \rangle$ average number of binary collisions per event,

$$R_{AA} = \frac{1}{\langle N_{bin} \rangle} \frac{\mathrm{d}^2 N_{AA}(p_T)/\mathrm{d}p_T \mathrm{d}y}{\mathrm{d}^2 N_{pp}(p_T)/\mathrm{d}p_T \mathrm{d}y}. \tag{1.1}$$

If the nuclear modification factor is equal to unity, $R_{AA} = 1$, no medium effects are observed. In d+A collisions, R_{AA} could be different from unity due to cold nuclear matter effects [2]. In central A+A collisions at maximum energy at RHIC and at LHC, R_{AA} is much less than 1. Suppression of J/Ψ in PHOENIX for different collision energies is shown in Fig. 1.2, the R_{AA} decreases with increasing number of participants N_{part} and is at lowest for the most central collisions.

The R_{AA} for heavy hadrons was predicted to be higher than for light hadrons due to smaller energy loss, but experimental observation revealed that the suppression for both kinds is about the same [10].

In what concerns heavy quarks, both charm and beauty quarkonia and open-charm suppression can be studied. In the deconfined medium, the presence of free colour charge is expected to screen the binding potential between the quark-antiquark pair. The larger the system is, the less it is bound and therefore breaks-off due to the colour screening more easily. Excited quarkonia systems are of larger size and weaker binding energy. Hence the spectral analysis of heavy-flavoured quarkonia could provide a QGP thermometer provided all other effects that influence the spectrum would be understood.

1.2.2 Jet quenching

Jets are highly collimated showers of partons originating from high-energy parton scattering, which occur during the initial stage of the collision [1]. The two partons that were initially scattered then travel in opposite direction. Should the scattering take place close to the surface of the fireball, one parton would then quickly leave the medium while the other one would have to travel through the formed plasma. Jet travelling through the hot matter would experience many collisions with the partons in the medium

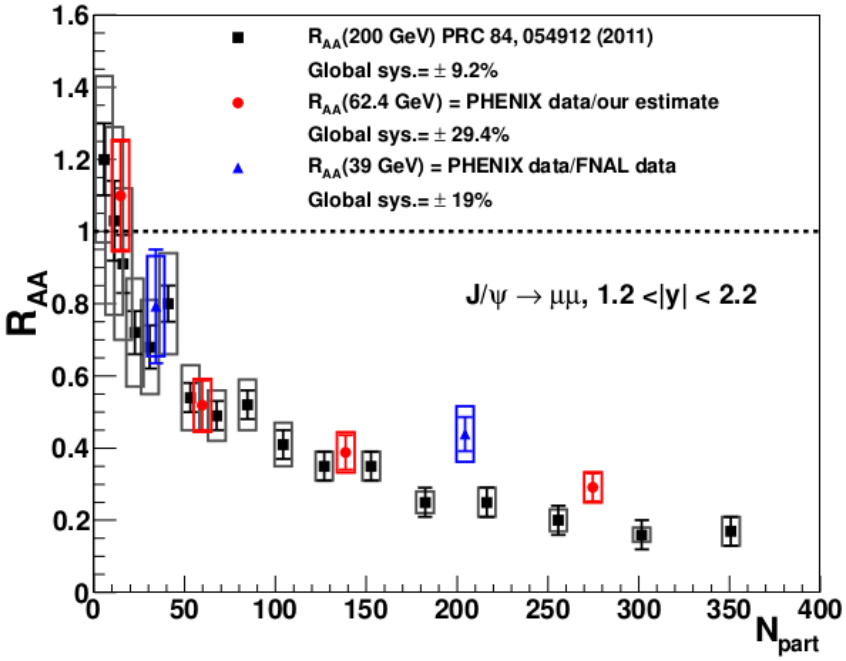

Figure 1.2: Suppresion of J/Ψ measured by PHOENIX for Au+Au at 39, 62.4 and 200 GeV. Taken from [6].

and would loose much more energy compared to the other jet. Such a phenomenon is refered to as *jet quenching*.

Figure 1.3 shows the azimuthal angular correlation function between the *trigger particle* and associated particles with lower momentum for p+p, d+Au and Au+Au at $\sqrt{s_{NN}} = 200$ GeV. Two peaks are clearly visible in p+p and d+Au collisions, one at $\Delta\phi = 0$ (near-side jet) and the other one at $\Delta\phi = \pi$ (away-side jet). No QGP is expected to form in these systems. However, in Au+Au collisions, the away-side jet vanishes. The explanation is that the jet undergoes many collisions with the partons inside the hot and dense matter and therefore looses most of its energy.

1.2.3 Collective flow

After nucleus-nucleus collision the pressure gradient in fireball leads to anisotropy in momentum of produced particles if system behaves collectively. The pressure gradient inside the system will create an additional boost to produced particles, usually refered to as *radial flow* [1]. In case the intial conditions were not spherically symetric (peripheral heavy-ion collisions, see Fig. 1.4a), one will observe the so called *anisortopic flow*. Asitropic and anisotropic flow are both visualised in Fig. 1.4b. The initial spatial anisotropy is converted into momentum anisotropy which can be measured.

The azimuthal anisotropy with respect to the reaction plane can be expressed in terms of a Fourier series

$$\frac{\mathrm{d}N}{\mathrm{d}\phi} = \frac{N}{2\pi}\left[1 + 2\Sigma v_n \cos\left(n(\phi - \Psi_R)\right)\right], \tag{1.2}$$

where ϕ is the angle of the particle with respect to reaction plane Ψ_R. The reaction plane is defined by the beam direction and by the vector connecting the centres of the two colliding nuclei. The Fourier

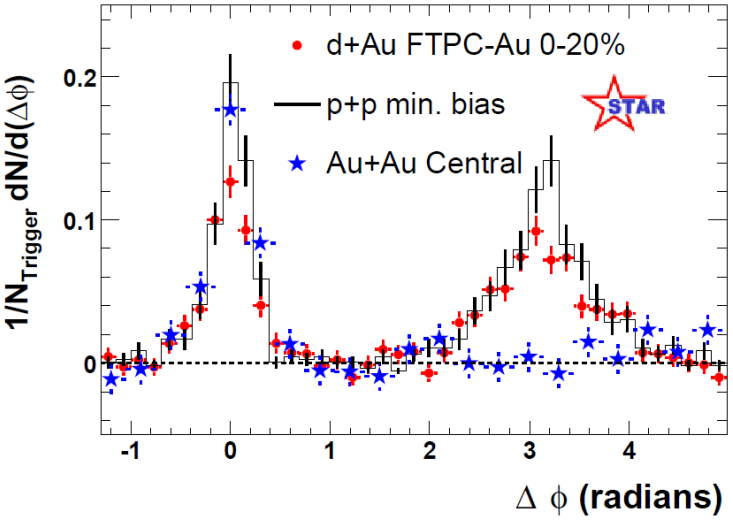

Figure 1.3: Distribution of particles with respect to the trigger particle (at $\Delta\phi = 0$) for p+p, d+Au and Au+Au at $\sqrt{s_{NN}} = 200$ GeV performed by STAR. The near-side jet ($\Delta\phi = 0$) is present for all systems. The away-side jet ($\Delta\phi = \pi$) is visible for p+p and d+Au only. Therefore we conclude that the away-side jet was absorbed while traversing the QGP. Taken from [3].

coefficients are defined as

$$v_n = \langle \cos n(\phi - \Psi_R)) \rangle \tag{1.3}$$

where the chevrons denote an average over all particles. Note that the first term in brackets in (1.2) describes the radial flow [7].

In heavy-quark measurements, the coefficient v_2 refered to as elliptic flow is of particular interest. In case of scenario of independent nucleon-nucleon collisions the quarks should be produced symmetrically and v_2 should be zero. On the other hand, strong v_2 could be consequence of collective hydrodynamical behaviour of created matter.Results for measurement of elliptic flow at RHIC can be found in Fig. 1.5.

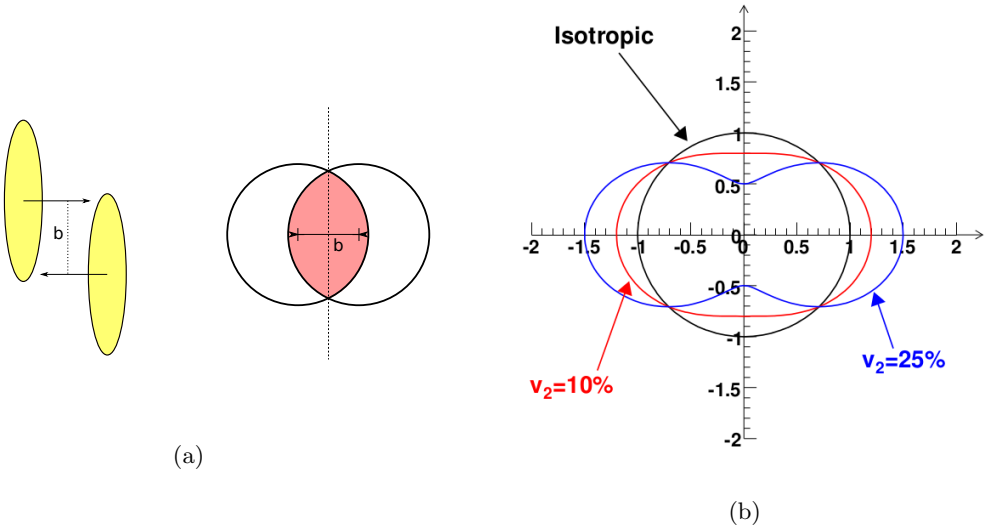

(a) (b)

Figure 1.4: (a) Schema of a peripheral heavy-ion collisions. The two nuclei collide with inpact parameter b. The overlap region is asymmetric and can be expressed as a function of b. (b) Profile of the particles emitted from the fireball, in the transverse plane. The x-axis in the figure coincide with the reaction plane. Taken from [4].

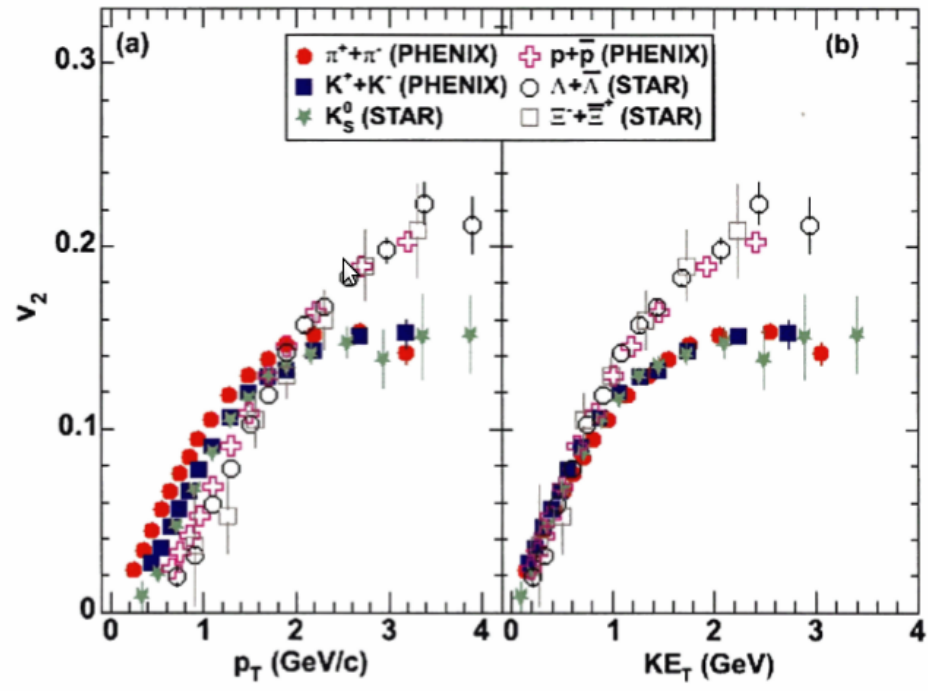

Figure 1.5: Elliptic flow for different species measured at RHIC as a function of (a) transverse momentum p_T and (b) transverse kinetic energy kE_T. Taken from [8].

Chapter 2

D^0 measurements at STAR experiment

Open charm measurements are an important part of investigation of heavy-quark production in ultrarelativistic nuclear collisions. They serve as an independent and complementary probe of the medium to J/Ψ measurements. In addition, open charm allows to measure the total charm cross-section.

In D^0 reconstruction, both hadronic and semi-leptonic channels can be used [10]. The semi-leptonic decay channel $D^0 \longrightarrow K^+ + l^- + \bar{\nu}_l$ has a higher branching ratio (9.6 %) and is easier to trigger. The drawbacks are an indirect reconstuction and contribution from both charm and bottom hadron decays. The hadronic decay $D^0 \longrightarrow K^- + \pi^+$ on the other hand suffers from a much smaller branching ratio of 3.89% of D^0 mesons.

2.1 Previous D^0 studies at STAR

Several open-charm measurements were carried on STAR data [2, 9, 10, 11]. D^0 and $\overline{D^0}$[1] production was previously investigated through hadronic decay$D^0 \longrightarrow K^- + \pi^+$ and $\overline{D^0} \longrightarrow K^+ + \pi^-$ in p+p at $\sqrt{s} = 200$ GeV[9] and $\sqrt{s} = 500$ GeV[10] and in d+Au and Au+Au at $\sqrt{s_{NN}} = 200$ GeV [11, 10]. The production in p+p data are consistent with upper limit of FONLL calculations [12], see Fig. 2.1.

In **p+p** at 200 GeV, D^0 were reconstructed in p_T region of $0.6 - 2.0$ GeV/c. The unsubtracted signal is shown in Fig. 2.2a. Two methods to determine combinatorial background were used - like-sign and rotational background. In both cases the residual background should be additionally subtracted. In this case the residual background was described by a second degree polynomial. Final signal for $p_T = 0.6 - 1.2$ GeV/c and $p_T = 1.2 - 2.0$ GeV/c can be found in Fig. 2.2b. The $\sqrt{s} = 500$ GeV dataset contained enough D^0 mesons in $0.6 - 2.0$ GeV/c p_T bin. The same technique as in the 200 GeV case were employed.

The **d+Au at 200 GeV** measurement lead to reconstruction of D^0 signal in transverse momentum region $p_T < 3.0$ GeV/c. Mixed-event technique was used for combinatorial background, residual background was approached through a linear function.

Finally, the **Au+Au at 200 GeV** data allowed to reconstruct D^0 signal over a p_T range of $0.0 - 8.0$ GeV/c, divided into seven p_T-bins. To obtain the raw signal, mixed-event background and second degree polynomial for residual background were employed. In Fig. 2.3, the invariance mass distribution

[1] In further text, by D^0 measurement, it is refered to both D^0 and $\overline{D^0}$. Relevant information concerning this issue will be explicitely stated.

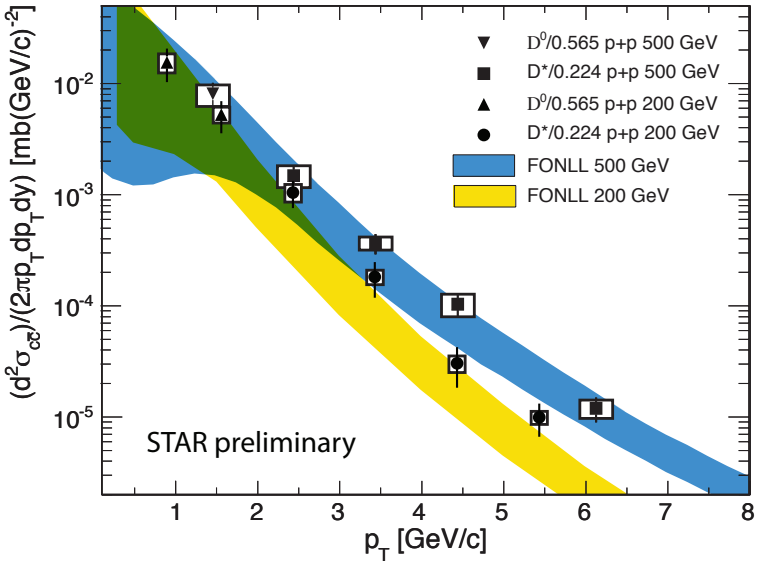

Figure 2.1: The invariant differential charm cross-section. The data are compared to pQCD FONLL calculation [12]. The FONLL upper limit describes the data well. Taken from [10].

before (a) and after (b) the background subtraction is displayed. The rightmost picture shows zoom of D^0 peak plus residual background (full circles) and only raw signal (open circles). The nuclear modification factor R_{AA} was then calcualted, see Fig. 2.4. The suppresion at high p_T is similar as for light hadrons.

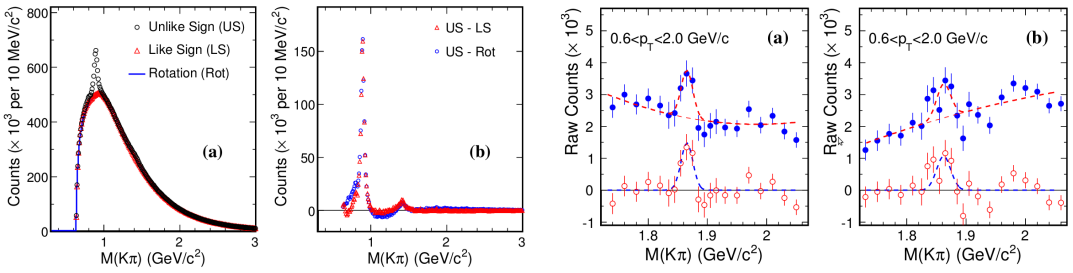

(a) (b)

Figure 2.2: D^0 reconstruction in p+p at $\sqrt{s} = 200$ GeV. (a) Invariant mass distribution for signal + combinatorial background (open circles) and for like-sign (triangles) and rotatinal (black line) background. The right plot shows invariant mass distribution after background subtraction, red for like-sign and blue for rotated. (b) Invariant mass distribution after background subtraction zoomed to the D^0 mass window, fitted by a sum of Gaussian and second degree polynomial function. Full circles show signal + residual background. Open circles show only signal. The Gaussian peak is drawn using the parameters obtained from fitting signal + res. background. Taken from [9].

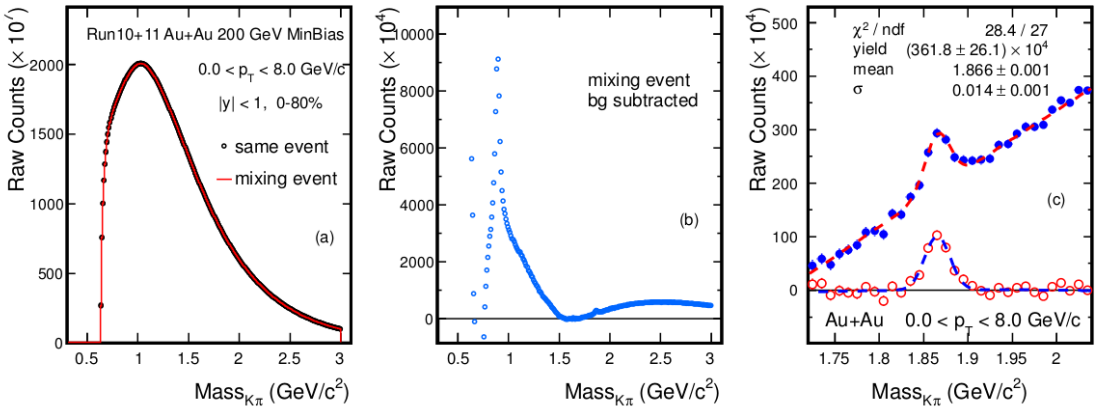

Figure 2.3: Invariant mass distribution for D^0 reconstructed from hadronic decay channel $D^0 \longrightarrow K^- + \pi^+$ in Au+Au at $\sqrt{s_{NN}} = 200$ GeV. (a) shows distribution before background subtraction. Red lines depicts mixed-event background used in this analysis. The situation after mixed background subtraction can be found in (b). The large peak was identified as $K^*()$ which also decays into $K^- + \pi^+$. The D^0 peak is clearly visible around $M_{K\pi} \sim 1.8$ GeV/c^2. The sum of raw D^0 signal and residual background is displayed in (c), full pictures, The situation after residual background subtraction is visualised by open circles. Taken from [10].

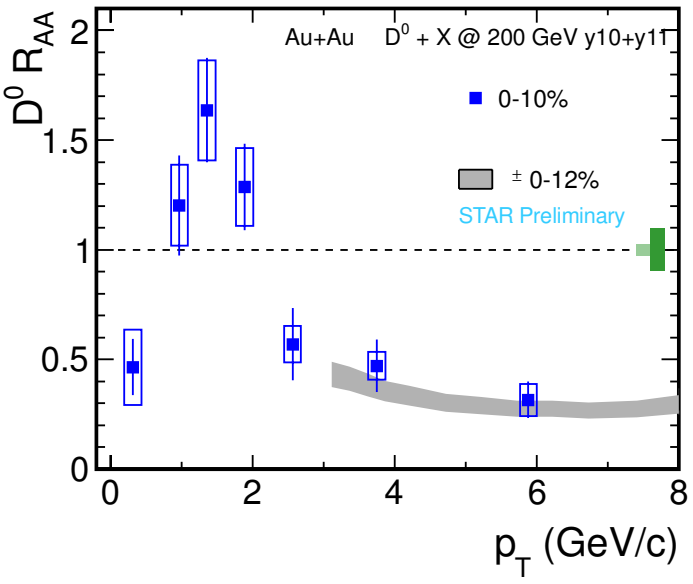

Figure 2.4: Nuclear modification factor R_{AA} for central Au+Au collisions. The suppresion at high p_T is similar to that in case of light hadrons. According to theoretical predictions, suppresion of heavy-flavoured hadrons was expected to be smaller. Taken from [10].

Chapter 3

STAR experiment at RHIC

3.1 The Relativistic Heavy-Ion Collider

The Relativistic Heavy-Ion Collider (RHIC) started its operation in 2000. The complex is located at the Brookhaven National Laboratory. Its main objective is to study the quark gluon plasma, the state at which all the matter is believed to have existed few seconds after the Big Bang [2].

The whole complex is shown in Fig. 3.1. The RHIC is an intersection ring with circumference of 3834 m, composed of two independent rings connected through six intersection points where particles collide. The experiments are therefore placed at these points. Originally, there were four experiments installed at RHIC: STAR, PHENIX, BRAHMS and PHOBOS. However, BRAHMS and PHOBOS had already completed their program. The RHIC performs both proton-proton and ion-ion collisions. Heavy-ions (d+Au, Cu+Cu, Au+Au, Cu+Au, U+U) are collided at centre-of-mass energies up to 200 GeV per nucleon-nucleon pair while the maximum centre-of-mass energy for proton-proton collisions is $\sqrt{s_{NN}} =$ 500 GeV. The fact that the two rings are independent enables the RHIC to collide asymmetric systems such as d+Au or Cu+Au.

Figure 3.1: Schema of the RHIC accelerator complex [13].

3.2 The STAR

The main physics goal of The Solenoidal Tracker at RHIC (STAR) is study of physical effects which occur under extreme conditions, namely production of quark gluon plasma. Undoubtedly the most important feature of the STAR is its full azimuthal coverage. Study of the azimuthal particle correlation is therefore possible. The coverage of rapidity is $|\eta| < 1.8$ [14].

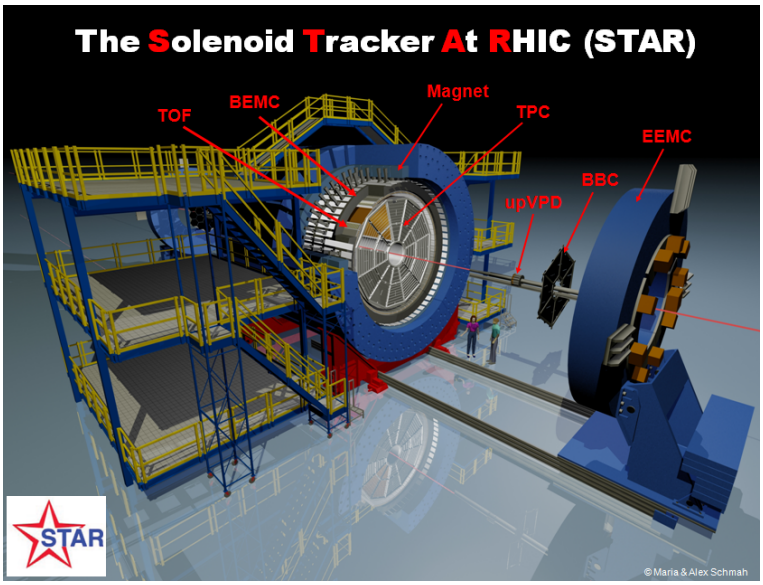

Figure 3.2: The STAR detector.

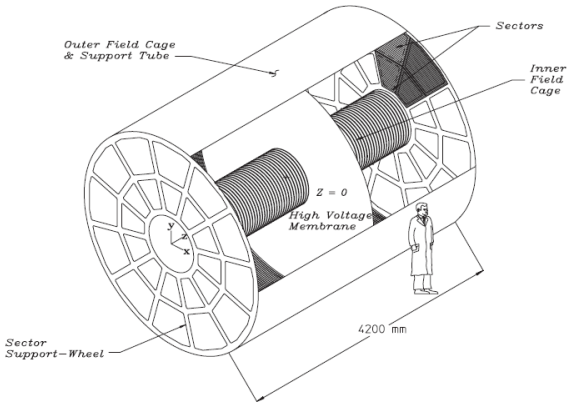

Figure 3.3: Schema of the TPC at STAR [14].

3.2.1 The Time Projection Chamber

The primary tracking device is the Time Projection Chamber (TPC). The TPC records tracks of produced particles, measures their momenta and their ionisation energy loss $\mathrm{d}E/\mathrm{d}x$ to identify the particles. TPC

Length of the TPC	420 cm
Outer Diameter of the Drift Volume	400 cm
Inner Diameter of the Drift Volume	100 cm
Distance: Cathode to Ground Plane	209.3 cm
Cathode Diameter	400 cm
Cathode Potential	28 kV
Drift Gas	90% Argon + 10% methane
Pressure	2 mbar above atmospheric
Drift Velocity	5.45 cm/μs
Signal to Noise Ratio	20 : 1
Magnetic Field	$\pm$ 0.5 T

Table 3.1: Basic parameters of the STAR TPC [14].

has the ability to measure wide range of particle momenta - from 100 MeV/c to over 30 GeV/c. Particles are identified up to 1 GeV/c.

The TPC is a cylindrical unit surrounding the beam-pipe (please see Fig. 3.2, the TPC itself is depicted in Fig. 3.3). The outer diameter is 4 m, the inner is 1 m. It has 4.2 m in length and is divided into two parts by a thin conductive Central Membrane (CM). The detector is seated in a large solenoidal magnet that operates at 0.5 T. The inner electric field is $\approx$ 135 V/cm. The CM is operated at 28 kV while the read-out caps are at ground. The volume is filled with a P10 gas (90 % argon, 10 % methane) regulated at 2 mbar above atmospheric pressure. The P10 gas has remarkably fast drift velocity which peaks at low electric field. The reason to operate at the peak of the velocity is that in such case the drift velocity remains stable even when subjected to small variations in temperature and pressure. Some of the basic parameters of the TPC are listed in Table. 3.1.

While passing the chamber filled with gas, particles ionise the gas. The ionisation produces secondary electrons. These then drift to the read-out caps. The read-out caps are split into 12 sectors. Each sector constitutes of several pad planes. The x and y coordinates of the track are reconstructed from the pad signal of drifting electrons hitting the cap. The z coordinate is calculated from the drift time of the electron cluster, travelling from its origin to the caps, combined with the average drift velocity.

The ionisation energy loss $\mathrm{d}E/\mathrm{d}x$ is given by the Bethe-Bloch formula

$$\frac{\mathrm{d}E}{\mathrm{d}x} = \frac{4\pi n_e z^2 e^4}{m_e \beta^2 c^2} \frac{1}{\beta^2} \left[ln \left(\frac{2 m_e c^2 \beta^2}{I(1-\beta^2)} \right) - \beta^2 \right] \tag{3.1}$$

where m_e is the electron mass, z is the atomic number of the target, β is the velocity of the incident electron, I is the mean excitation potential, n_e is the electron density in the target. Note that the energy loss per unit length is independent of the mass of the particle. Hence the velocity of the particle can be calculated without previous identification of the particle, e. i. without knowing its mass. However, momenta are used to identify particles rather than their velocities. A typical plot of $\mathrm{d}E/\mathrm{d}x$ versus momentum is shown in Fig. 3.4.

The momentum can be found from cyclotron equation

$$p = qBR \tag{3.2}$$

where p is the momentum of the particle with charge q, B is the magnitude of external magnetic field and R is the radius of particle' s curvature. The uniform magnetic field within the TPC is $|B| < 0.5$ T The charge is assumed to be $q = \pm 1e$.

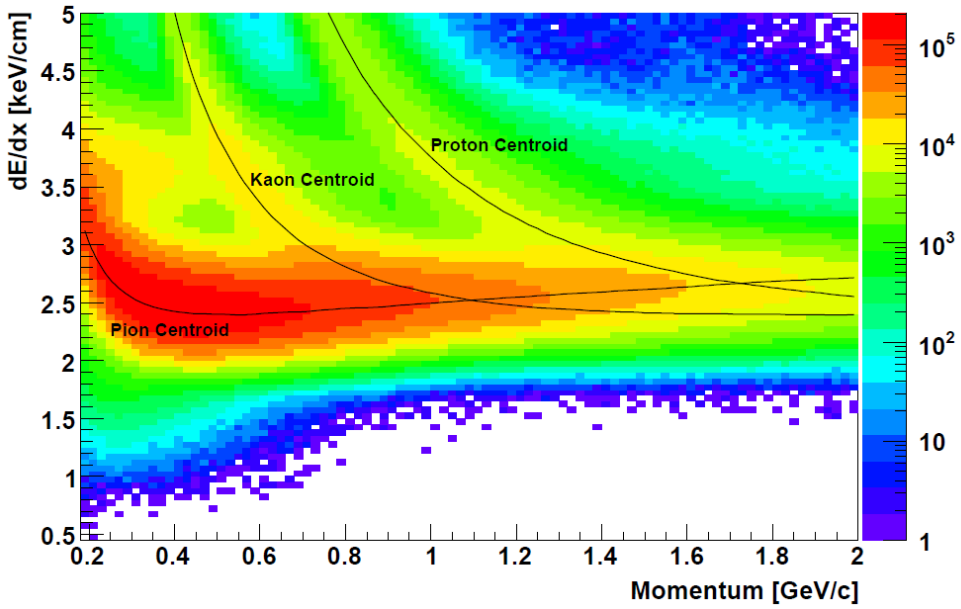

Figure 3.4: A typical plot of $\mathrm{d}E/\mathrm{d}x$ versus momentum from data from TPC [14].

3.2.2 The Time of Flight

The Time of Flight (TOF) is a barrel detector with a full coverage in azimuthal angle and with $|\eta| \leq 1$. With resolution under ~ 100 ns and high detection efficiency ($> 95\%$), it increases particle identification efficiency of the STAR. Kaons and protons can be separated from pions up to ~ 1.7 GeV/c and up to ~ 3.0 GeV/c respectively. The TOF detector is very important in D meson measurement, since it reduces combinatorial background of the daughter particles by factor 3 and greatly reduces required beam-time, thus making these measurements feasible [15].

The capability of STAR to identify particles can be enhanced by combined use of the TPC and of the Time of Flight (TOF). The TOF measures particles velocity β. When used together with particle' s momentum p from TPC, both pieces of information serve to calculate particle' s mass m as

$$m = p\sqrt{1/\beta^2 - 1} \tag{3.3}$$

The TOF measures start times and stop times of the tracks. The velocity β is found by dividing the path length L of the particle from the event vertex to the TOF by the time necessary to traverse this path length Δt

$$\beta = \frac{L}{c\Delta t} \tag{3.4}$$

The TOF consist of two subdetectors – pVPD ("start" detector) and TOF ("stop" tray detector). The TOF is situated directly in the STAR magnet, as it sits outside the TPC (see Fig. 3.5). Its operation is based on Multi-gap Resistive Plate Chamber (MRPC) technology. The MRPC can be described as stack of resistive glass plates, separated by miniscule gaps. A passing charged particle ionisates the gas in the gaps. The ionisation effect is amplified by the high voltage applied to the external surfaces of the chamber. Once the particle has passed through the gap, the resisitve glass plates quench the avalanche. There is thus no " late tale" in the signal. The signal is a sum of signals from multiple gaps.

The detector is set close to the Geiger mode, which means the ionised gas discharges and then quenches very quickly. Hence the resolution of the TOF.

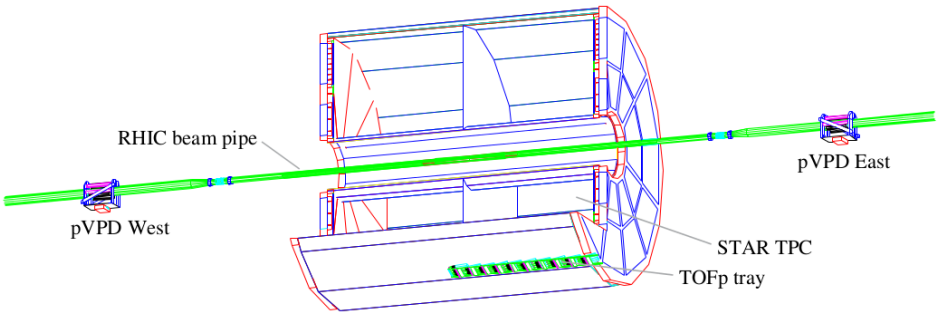

Figure 3.5: Schema of the TOF and pVPD subsystems. The TOF is situated outside the TPC. Only one tray is shown in this picture. The pVPD detectors are situated outside the magnet, both at the same distance from the centre of the detector. Taken from [15].

The pVPD stands for Pseudo-Vertex Position Detector and it is a set of two detectors, wrapped around the beam-pipe on both sides of the STAR chamber. In nucleus-nucleus collisions, there are prompt energetical photon pulses travelling in the direction of the original beams. pVPDs measure the time at which these pulses reach them. The average of these two times t_1 and t_2

$$t_{start} = \frac{t_1 + t_2}{2} \tag{3.5}$$

is then the start time for the TOF detector.

Chapter 4

D^0 production at STAR in U+U collisions at $\sqrt{s_{NN}} = 193$ GeV

It is impossible to directly observe open charm hadrons with STAR detector. They do decay before reaching the detector (in case of D^0, $c\tau = 122.9$ μm). Therefore it is necessary to reconstruct charm hadrons through their decay products. In case of $D^0 \longrightarrow K^- + \pi^+$ and $\overline{D^0} \longrightarrow K^+ + \pi^-$, the daughter particles are easily idetnified using the TPC and the TOF. However, as it is a rather rare process (B. R. of 3.89%), the channel used for this analysis suffers from large combinatorial background. Therefore a set of various selection criteria were necessary to improve the signal to background ratio. For better statistics, we inspected signal in sum of both D^0 and $\overline{D^0}$ decays $D^0 + \overline{D^0}$[1].

Important D^0 characteristic are summed up in Tab. 4.1.

D^0	M_D [GeV/c^2]	$c\tau$ [μm]	B.R.($D^0 \longrightarrow K^- + \pi^+$)
$(c\bar{u})$	1.8645 ± 0.0004	122.9	3.89%

Table 4.1: Important characteristics of D^0 meson: quark composition, mass, lifetime, branching ratio of $D^0 \longrightarrow K^- + \pi^+$ channel [16].

4.1 Event and Track Selection

Data taken during 2012 U+U runs were processed during the analysis here described. Total of 320 minimum-bias events were preselected before tha actual analysis using a set of cuts described bellow. An overview of these cuts can be found in Tab. 4.2.

|Vz – VpdVz|	< 2.25 cm
|VertexZ|	< 40 cm
Event Multiplicity	> 10
must contain $K\pi$ pair	

Table 4.2: Cuts used for D^0 analysis in U+U data.

[1] Further in the text, we will refer to this only as D^0

The first condition in Tab. 4.2 serves as a prevention of so called pile-ups. The TPC is a slow detector and hence it reads out data from many bunch crossing. Therefore different tracks from different primary vertices might be mixed together. The VPD, on the other hand, is a very fast detector. It can therefore "see" events from single crossings. This cut ensures that only tracks from events identified by both VPD and TPC are accepted. The distribution of $|Vz - VpdVz|$ can be seen in Fig. 4.1a

The second requirement applies to vertex position along the beam-line, see Fig. 4.1b. This cut prevents bias from high-material region [2].

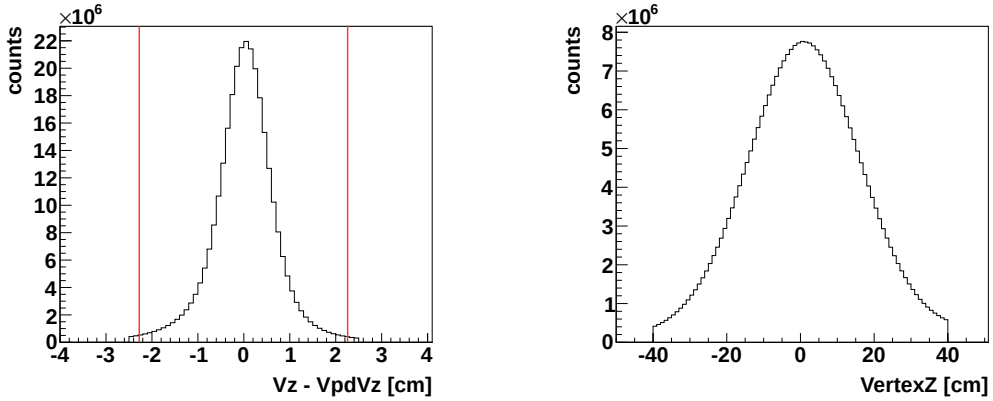

(a) (b)

Figure 4.1: (a) Distribution of $|Vz - VpdVz|$ in U+U at $\sqrt{s_{NN}} = 200$ GeV. The applied cut is visualised by red lines.(b) Distribution of Vz position in U+U data at $\sqrt{s_{NN}} =$ GeV.

The reference multiplicity cut-off leaves out the most peripheral collisions. This quantity is related to the centrality of the collision. The higher the reference multiplicity, the more central is the corresponding collision. Centrality clases for U+U collisions were not yet defined at time when analysis was carried. Reference multiplicity distribution for U+U data is shown in Fig. 4.2a.

The cut on DCA (Distance of Closest Approach) ensures that the two particles come from the same vertex. Most tracks fall within used cut, see Fig. 4.2c. Particles have to have a certain minimal value of transverse momentum to be accepted, see Fig. 4.2b. Another important criterion is the *number of* TPC *hits*. Tracks are reconstructed in TPC from registered hits - therefore the higher the number of hits, the more precise is the final track. Only tracks reconstructed from more than 19 points were kept, hit-number distribution together with the applied cut is in Fig. 4.2d.

The condition on pseudorapidity means that the tracks would be within acceptance of the TPC and of the TOF. Pseudorapidity distribution is in Fig. 4.3a. The cut on rapidity of original open charm meson is used for the same reason.

The TofLocalY cut (Fig. 4.3b) is used to prevent TOF pile-ups. A TOF read-out pad is shown in Fig. 4.4. The TofLocalY variables gives distance from centre of the pad in Y direction (horizontal). By restricting the maximal value accepted, events with particle hiting in between two pads or very close to the pad borders are excluded. Signal from such tracks might be read-out by both pads, making it impossible to tell the real path of the particle.

4.1.1 PID Cuts

In the current analysis, daughter particles were identified by combined use of TPC and TOF. TPC cuts were employed over a momentum range of $p \in [0.2; 0.6]$ GeV/c and > 3.0 GeV/c. The $\mathrm{d}E/\mathrm{d}x$ for pions,

D^0 reconstruction cuts	
|VertexZ|	< 40 cm
|VerteZ – VpdVertexZ|	< 2.25 cm
Event Multiplicity	$\geq$ 10
p_T	≥ 0.2 GeV/c
DCA	≤ 2 cm
# TPC Hits	≥ 20
$\|\eta\|$	< 1
|TofLocalY|	< 1.8 cm
$\|y(D^0)\|$	< 1
PID – TPC	
p_T	$\in [0.2; 0.6]$ or > 3.0 GeV/c
$\|n_\sigma\|$	< 2
PID – TOF	
p_T	$\in [0.6; 3.0]$ GeV/c
$\|n_\sigma\|$	$= f(p)$

Table 4.3: List of selection criteria. The TPC

kaons and protons is displayed in Fig. 4.5 left. Coloured lines represent Bichsel function calculated for single particle species. It is assumed that particles are gaussian distributed around the central value. The pion band is without kaon or proton contamination up to $p \sim 0.6$ GeV/c. However at $p = 0.6-3.0$ GeV/c the three bands overlap and it is very difficult to correctly identify particle species. At $p > 3.0$ GeV/c, the pion and kaon bands should be already separated. The kaon band is however slightly contaminated by protons. We assume this contamination is not much affecting our results. Hence we excluded TPC cuts in the momentum window of $p = 0.6 - 3.0$ GeV/c. In this range, we used TOF cuts instead.

The $n\sigma$ gives the number of standard deviations from the central value and is defined as

$$n\sigma = \frac{\ln \mathrm{d}E/\mathrm{d}x_{th} - \ln \mathrm{d}E/\mathrm{d}x_{meas}}{R}, \tag{4.1}$$

where the $\mathrm{d}E/\mathrm{d}x_{th}$ and $\mathrm{d}E/\mathrm{d}x_{meas}$ represent calculated and measured ionisation loss respectively and R is detector resolution. We set

$$|n\sigma_\pi| < 2, \tag{4.2}$$

and

$$|n\sigma_K| < 2. \tag{4.3}$$

Particles left after the cut are shown in Fig. 4.5 right.

The TOF system was used to identify single species in the $0.6-3.0$ GeV/c momentum window. Again, gaussian distribution is assumed. The $1/\beta$ vs p distribution is shown in Fig. 4.6 left. The central value is calculated as

$$\frac{1}{\beta}_{th} = \sqrt{\frac{m^2}{p^2} + 1} \tag{4.4}$$

where m and p is mass and momentum of a particle respectively. Only particles fulfilling a 2σ cut were accepted. The condition reads

$$\frac{1}{\beta} \in \left[\sqrt{\frac{m^2}{p^2} + 1} - 2\sigma_X; \sqrt{\frac{m^2}{p^2} + 1} + 2\sigma_X \right] \tag{4.5}$$

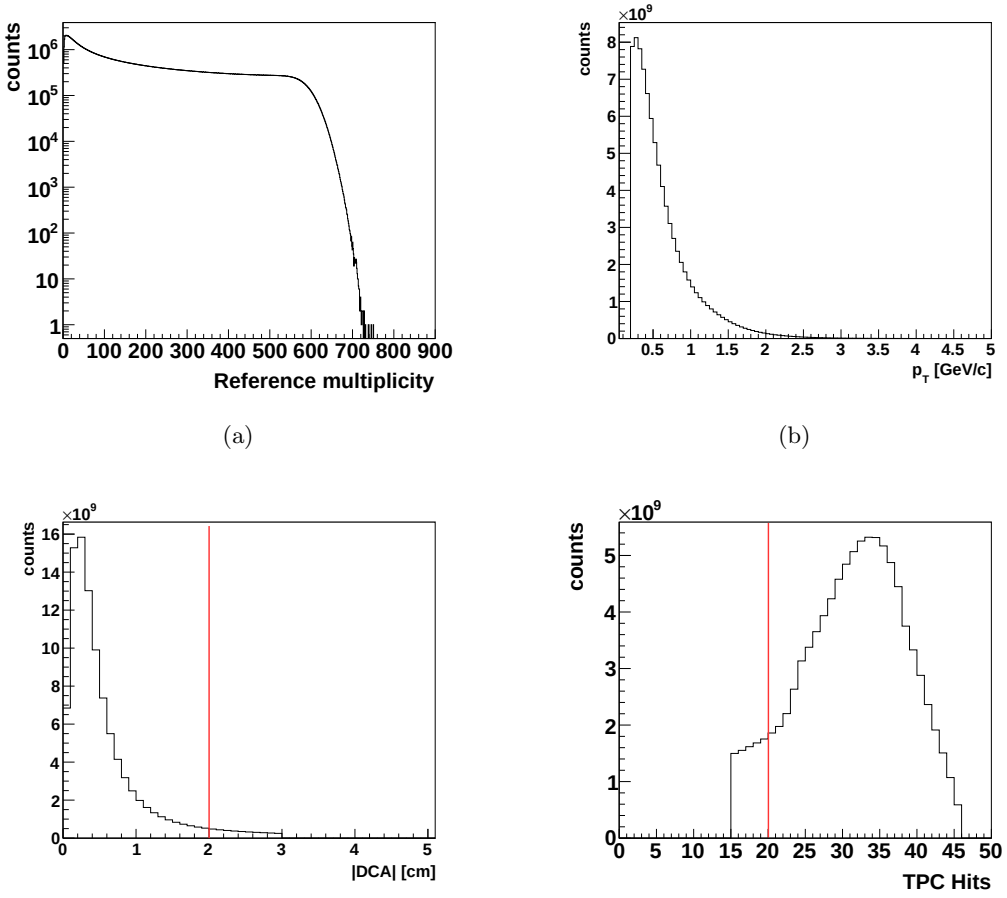

Figure 4.2: (a) Reference multiplicity in U+U at $\sqrt{s_{NN}}$ = 200 GeV. The most peripheral collisions were omitted.(b) p_T distribution in U+U data at $\sqrt{s_{NN}}$ = GeV. (c) DCA for U+U at $\sqrt{s_{NN}}$ = GeV minimum-bias dataset. (d) Distribution of number of TPC its for U+U data.

where σ_X stands for standard deviation for single species distribution. In current analysis, we set

$$\sigma_K(p) = 0.0076 + \frac{0.0014}{1.89^{1.758p} - 1.152^{1.57}} \tag{4.6}$$

in the case of kaons and

$$\sigma_\pi = 0.0075 \tag{4.7}$$

for pions.

It is well visible that TOF is able to perfectly separate pions from kaons up to $p \sim 1.6$ Gev/c. As the TOF PID cuts were applied up to 3.0 GeV/c, particles with $p > 1.6$ GeV/c might get misidentified. The same problem might have arosen with pions and kaons identified with TPC. Therefpre it is necessary to carry a double-counting estimation. This subject is addressed in Sec. 4.3.

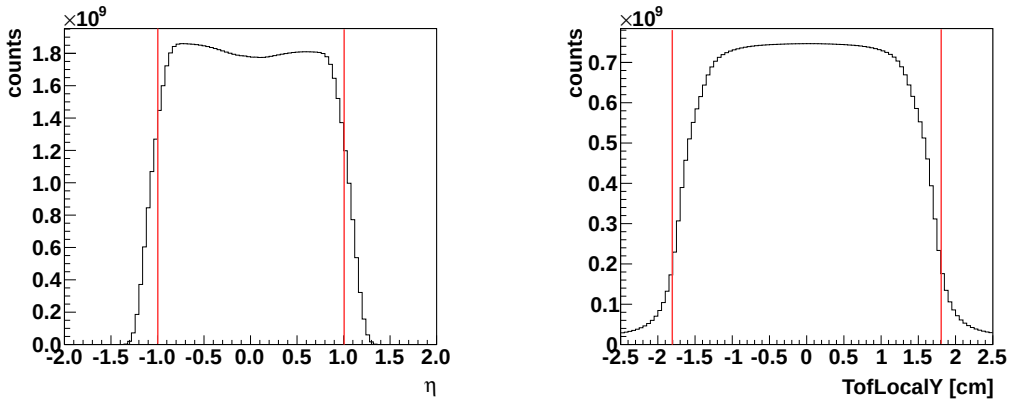

(a) (b)

Figure 4.3: (a) Pseudorapidity distribution for U+U at $\sqrt{s_{NN}}$ = GeV. (b) TofLocalY distribution for the same dataset. The cut (red lines) prevents TOF pile-ups.

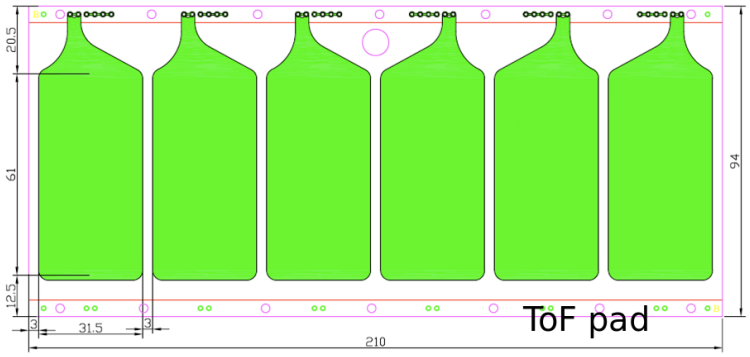

Figure 4.4: Schema of TOF sector with read-out pads. Charge deposited in between teo pads would be read-out by the two pads and might cause pile-ups.

4.2 D^0 reconstruction

The open charm hadrons are reconstructed from their decay products by calculating the invariant mass of the $K\pi$ pair. From conservation of momentum and energy, the invariant mass is given as

$$M_{K\pi} = \sqrt{(E_K + E_\pi)^2 - (p_K + p_\pi)^2}. \tag{4.8}$$

As most of the $K\pi$ pairs do not come from $D^0 \longrightarrow K^- + \pi^+$ decay, one has to deal with a huge combinatorial background. The invariant mass distribution integrated over $p = 0.0 - 5.0$ GeV/c can be found in Fig. 4.7. No clear peak around the D^0 mass region is visible. Therefore we have to implement methods to describe this combinatorial background of randomly formed pairs. We will discuss three possible methods: rotational bakground, like-sign background and mixed-event background.

In the first method, one of the particles is rotated so that its momentum is pointing in opposite

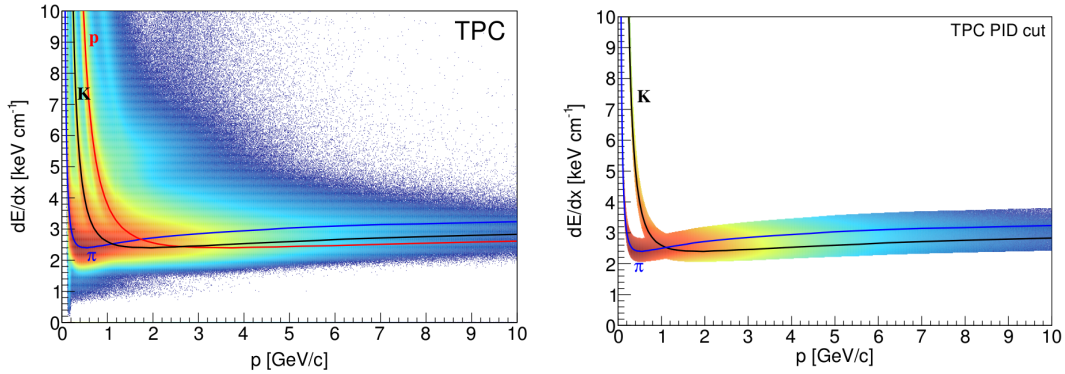

Figure 4.5: (Left) dE/dx vs p in minimum-bias U+U at $\sqrt{s_{NN}} =$ GeV. Bichsel parametrisation for pions (blue), kaons (black) and protons (red) are shown. Gaussian distributions are assumed. (Right) The 2σ pion and kaon cut.

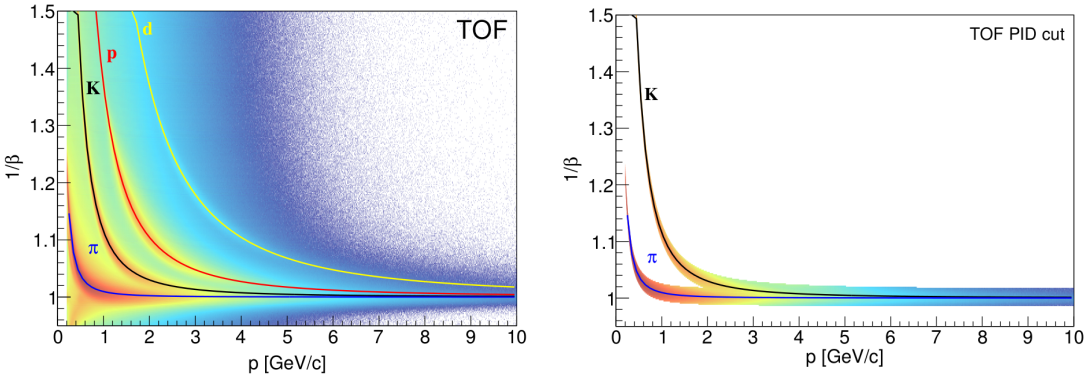

Figure 4.6: (Left) 1β vs p in minimum-bias U+U at $\sqrt{s_{NN}} =$ GeV. Gaussian distributions are assumed. Central values for pion (blue), kaons (black), protons (red) and deuterons (yellow) are visible. (Right) The 2σ pion and kaon cut for TOF.

direction,

$$(E, p_x, p_y, p_z) \longrightarrow (E, -p_x, -p_y, -p_z), \tag{4.9}$$

thus destroying all correlation.

Another technique uses pairs of same sign. This method is suitable for decays, where the two products are of oppposite sign, which is the case of D^0. Using this technique garantees reconstruction of trully random pairs originating from the same event. Combining pairs from events with very different geometry might cause additional problems [2]. On the other hand, it ensures that the particles do not come from one decay.

As last, we shall mention the event-mixing method. Particles from different, yet similar events (i. e. from the same centrality class) are combined to obtain invariant mass dsitribution. Hence no correlation between the daughters takes place. In analysis here presented, one kaon(pion) from one event was combined with 5 pions (kaons) from different events with similar geometry. The main advantage of this method is the large statistics, contrary to the two previously mentioned techniques.

In further text, only the mixed-event bakground is used for combinatorial background description.

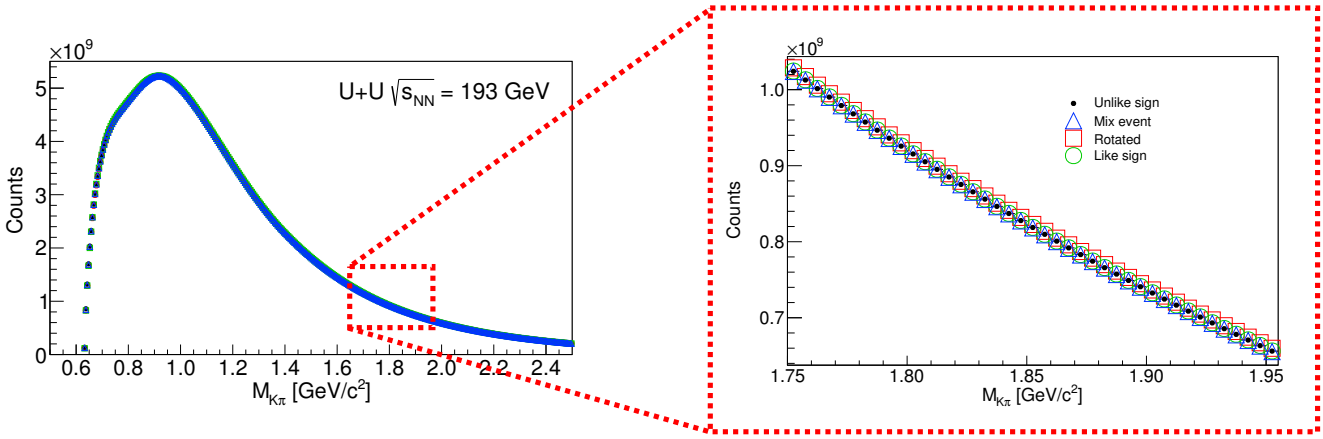

Figure 4.7: Invariant mass distribution for $K^{\pm}\pi^{\mp}$ pairs in U+U at $\sqrt{s_{NN}} =$ GeV. Unlike-sign (black), like-sign (green), rotated (red) and mixed-wvent (blue) background. The zoom displays the D^0 mass region. Due to large combinatorial background, no signal is yet visible.

The invariant mass distribution after mixed-event background subtraction integrated over transverse momentum range of $0.0-5.0$ GeV/c^2 is displayed in Fig. 4.8. A peak at the position corresponding to D^0 mass $m_D = 1.864$ GeV/c^2 [16] is clearly visible over the residual background. The residual background results from e. g. misidentified resonances, overlaping decay channel from the same mother particle or jets [2]. Signal and background were described making use of sum of Gaussian and second degree polynomial function. The significance of the signal was calculated as

$$sg = \frac{S}{\sqrt{S+B}}. \tag{4.10}$$

For the D^0 signal, $sg = 6.4\ \sigma$.

The structure around $M_{K\pi} \sim 0.7 - 1.0$ GeV/c^2 has several possible sources. The tall peak around 0.9 GeV/c^2 originates from decay of $K^*(892)$. Another possible explanation is misidentification of one of the decay products, thus resulting in shifted invariance mass.

The integrated invariant mass was divided into 5 p_T-bins (see Fig. 4.9) in order to see the extent of the signal. Raw yields and significances of D^0 signal for each bin are summed in Tab. 4.4.

p_T [GeV/c]	Raw Yield ($\times 10^3$)	significance
$0.0 - 0.6$	117 ± 31	3.8
$0.6 - 1.1$	203 ± 68	3.0
$1.1 - 1.8$	189 ± 58	3.3
$1.8 - 3.0$	167 ± 44	3.8
$3.0 - 5.0$	65 ± 19	3.4

Table 4.4: D^0 raw yield and significance for each bin over the p_T range $0.0 - 5.0$ GeV/c.

It is still necessary to determine various corrections factors to obtain the corrected yield. One of those corrections involve double counting estimation. The double-counting estimation was performed for this analysis and is discussed in next section.

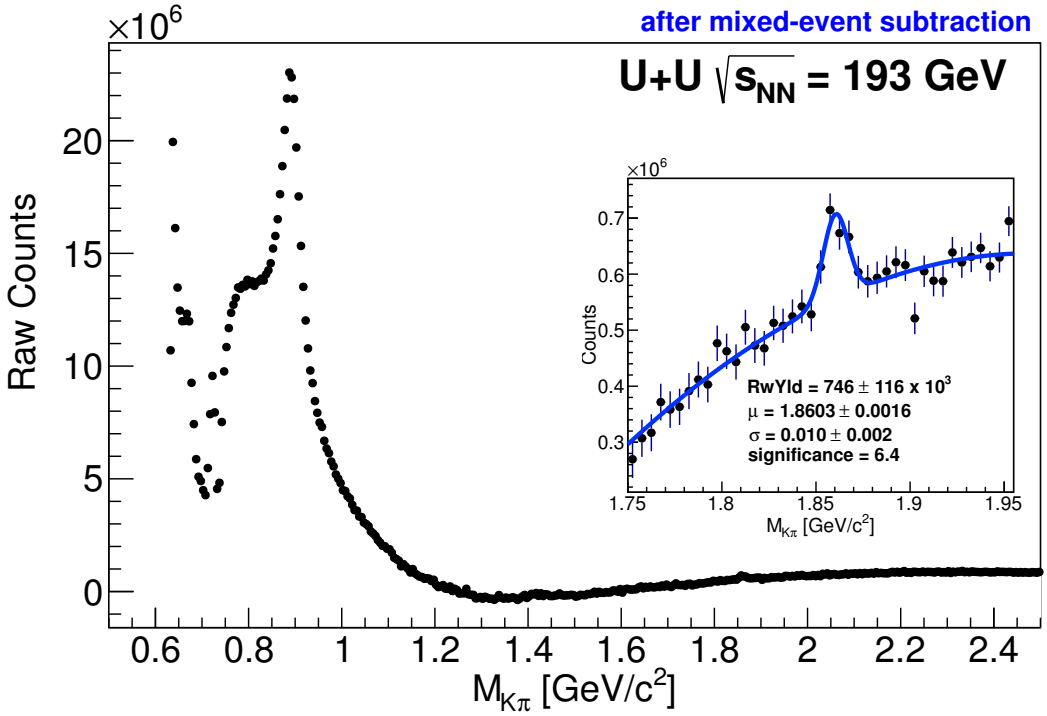

Figure 4.8: Invariant mass distribution for $K^{\pm}\pi^{\mp}$ pairs in U+U at $\sqrt{s_{NN}} =$ GeV after mixed-event background subtraction. Integrated over $0.0 - 5.0$ GeV/c transverse momentum region. A peak around $M_{K\pi} \sim 1.86$ GeV/c^2 is visible over the residual background. The peak at $M_{K\pi} \sim 0.8$ GeV/c^2 comes from decay of $K^*(892)$.

4.3 Double-counting estimation

In D^0 reconstruction, daughter particles might get misidentified. Kaon is then labeled as pion and vice-versa. In such case, the pair will contribute to both D^0 and $\overline{D^0}$ signal. Therefore it is important to determine the rate of such misidentification in the D^0 analysis. Double counting ratio in D^0 reconstruction here presented was estimated with use of Monte Carlo simulation.

The method consists of three consecutive steps:

- determination of particle missindentification probability based on TPC and TOF PID resolutions extracted from real data,
- generation of sets of kaons and pions followed by D^0 reconstruction,
- calculation of ratio of D^0 from misidentified daughter particles to all D^0.

All steps will be described in detail in the following text.

The particle misindentification probability

For both TPC and TOF PID, gaussian distribution of particles is assumed. The central $\langle \mathrm{d}E/\mathrm{d}x \rangle$ value were calculated from Bichsel function, 2σ band and resolution of 8% were considered. The TOF PID central values were obtained from (4.4). The "2σ" cut to determine wheather the particles should be still considered as kaon or pion is given by (4.6) and (4.7) respectively. Given these distributions, fraction of kaons (pions) that fall into the pion (kaon) band was estimated. The fraction represents the misidentification probability, which is shown in Fig. 4.10.

Particle MC generation

As next, 500 million of D^0 particles of mass $M_D = 1.8645$ GeV/c^2 were generated using Monte carlo with uniformly distributed random values of azimuthal angle $\phi \in [0; 2\pi]$, rapidity $y \in [-1; 1]$ and a powerlaw p_T distribution for $p_T \in [0; 10]$ GeV/c. The particle is given as a four-vector

$$D^0 = (p_T; \eta; \phi; M_D) \tag{4.11}$$

where the pseudorapidity η is calculated from generated quantities. Kaons and pions were then randomly generated in the D^0 rest-frame again with uniformly distributed random values of azimuthal angle $\phi' \in [0; 2\pi]$ and with $\cos\theta' \in [-1; 1]$. The absolute value of their momenta was given as

$$p' = \frac{1}{2M_D}\sqrt{[M_D^2 - (m_\pi - m_K)^2][M_D^2 + (m_\pi - m_K)^2]}.$$

Other necessary kinematic quantities can be calculated from these values and the kaon and pion four-vectors are given as

$$K = (p'_T; \eta'; \phi'; m_K)\,, \tag{4.12}$$

$$\pi = (p'_T; -\eta'; \phi' + \pi; m_K)\,. \tag{4.13}$$

Then, both the kaon and pion four-momentum were transformed to the laboratory frame and smeared by Gaussian and the final D^0 candidates were reconstructed. Those not fulfilling the condition $|y_D| < 1$ and not falling into the 2σ mass and transverse momentum windows were omitted and number of all reconstructed D^0 was determined. Number of misidentified kaons and pions were estimated using the misidentification probabilities calculated earlier in the process. Then again, D^0 candidates from these misidentified daughters were reconstructed applying the same conditions.

The two distributions are shown in Fig. 4.11. The left plot contains all reconstructed D^0 mesons. The right plot shows candidates obtained from misidentified daughters. We can already conclude from these plots that the double counting takes place for $p_T \geq 3$ GeV/c.

Ratios of misidentified particles

Finally, p_T distributions of all and misidentified D^0 candidates lying in $1.82 - 1.90$ GeV/c^2 mass region were produced (visualised by dot-and-dashed lines in Fig. 4.11). The double counting fractions were then calculated as

$$\frac{\mathrm{d}N/\mathrm{d}RcM_{Dmis}}{\mathrm{d}N/\mathrm{d}RcM_D}. \tag{4.14}$$

The result is shown in Fig 4.12. Open circles and blue stars represent double counting ratios in case only TPC and TOF cuts are applied, respectively. Red triangles show the ratio for the combination of TPC and TOF as was used in analysis here presented. Up to $p_T = 3$ GeV/c, there is no double-counting contamination of the signal. In $3 < p_T < 10$ GeV/c region, the double-counting ratio does not exceed 10%. The double counting probability in the lower p_T region ($0.0 - 3.0$ GeV/c) is visibly dominated by TOF. Then it starts to grow, but up to $p_T \sim 6.0$ GeV/c, the ratio is lower then if only TPC or only TOF were used. At hugher p_T, the probability estimation is fully drawn by TPC. Therefore we can conclude, that the cuts described in 4.1.1 result in lower double counting contamination than of we used only one of the two subdetectors at a time.

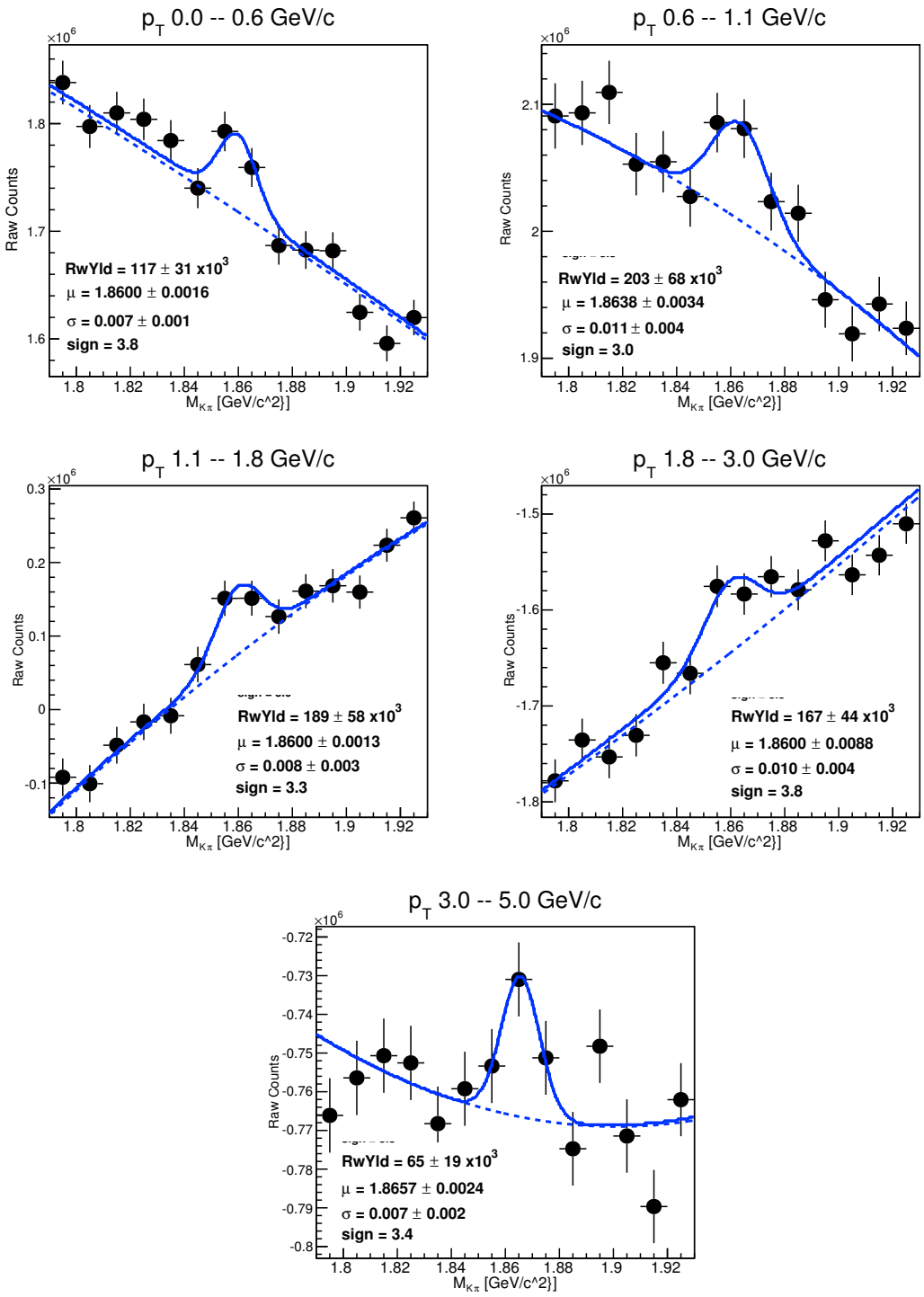

Figure 4.9: Invariant mass distribution for $K^{\pm}\pi^{\mp}$ pairs in U+U at $\sqrt{s_{NN}}$ = GeV after mixed-event background subtraction. The signal was divided into 5 p_T-bins covering the transverse momentum range of $0.0 - 5.0$ GeV/c. The residual background is described by a second degree polynomial.

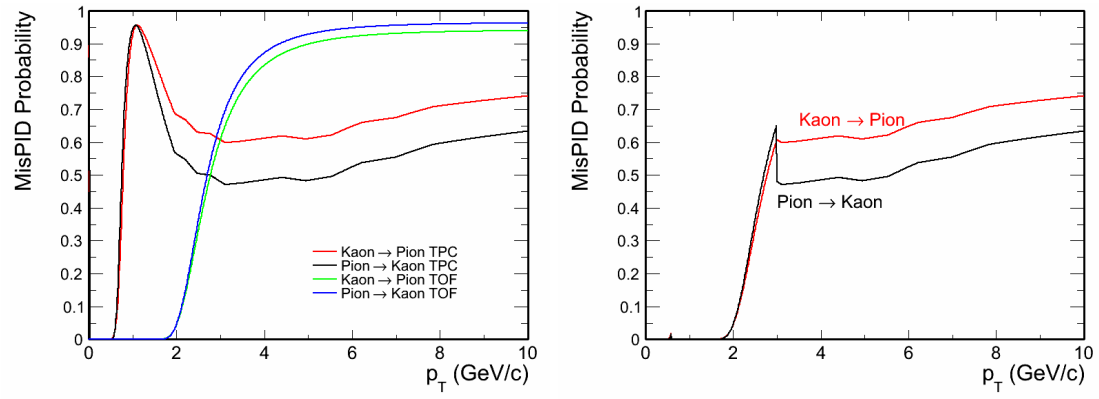

Figure 4.10: Particle misidentification probability for kaons and pions in D^0 reconstruction. The left figure represents misidentification probabilities for TPC PID (red and black) and TOF PID (blue and green). The probability corresponding to PID cuts used in current analysis is shown on right.

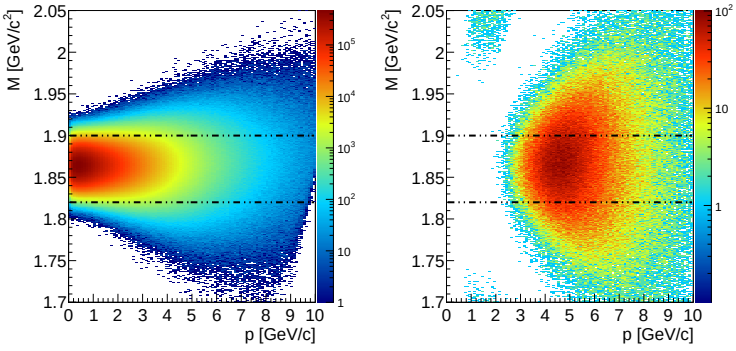

Figure 4.11: Distribution of D^0 candidates from all particles (left) and from misidentified daughter. The colour scale is different for each plot.The dot-and-dashed lines represent the D^0 mass region $M = 1.82 - 1.90$ GeV/c^2

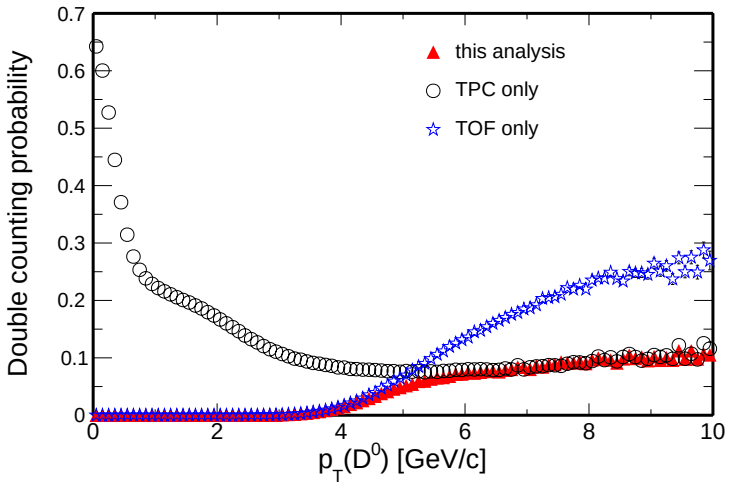

Figure 4.12: The D^0 double counting probability for the UU analysis. Open circles represented double counting when only TPC cuts are applied, blue stars for when only TOF is used. The PID cuts used for current analysis result in double counting visualised by red triangles.

Summary

Study of charm mesons can unveil information about the new state of matter created in ultrarelativistic heavy-ion collisions. Due to their large mass, charm quarks are expected to interact differently with the hot and dense medium than light quarks. Open charm studies serve as an complementary measurement to J/Ψ measurement and contribute to the total charm cross-section. Production of open charm meson D^0 was previously measured by STAR in p+p, d+Au and Au+Au systems.

In this work, we presented status of analysis of open charm meson through hadronic decay $D^0 \longrightarrow K^- + \pi^+$ and $\overline{D^0} \longrightarrow K^+ + \pi^-$ in U+U collisions at $\sqrt{s_{NN}} = 193$ GeV at STAR experiment. Daughter particles were identified applying set of conditions on data recorded by TPC and TOF. Combanatorial background was estimated through mixed-event method. $D^0 + \overline{D^0}$ candidates were reconstructed up to $p_T = 5.0$ GeV/c with significance larger than or equal to 3σ.

These raw results need to be corrected due to several effects that might affect total count. Several factors have to be taken in account. Double counting estimation was performed for our data and selection criteria. Several daughter particles could have been misidentified in one of the subdetectors. Such misidentified pairs would then contribute twice to the total signal. Our study implies that the signal is not affected by double counting up to $p_T = 4.0$ GeV/c. In higher p_T region it does not exceed 10 %.

Bibliography

[1] S. Sarkar, H. Satz, B. Sinha (Eds.), *The Physics of the Quark-Gluon Plasma: Introductory Lectures*, Lect. Notes Phys. 785, Springer, Berlin Heidelberg 2010.

[2] S. Baumgart, PhD Thesis, Yale University 2009.

[3] J. Adams *et al.* (STAR Collaboration), Nucl. Phys. **A 757**, 102-183 (2005).

[4] E. Bruna, PhD Thesis, University of Torino 2007.

[5] G. Eyyubova, PhD Thesis, University of Oslo 2013.

[6] A. Adare *et al.* (PHENIX Collaboration), Phys. Rev. **C 86**, 064901 (2012).

[7] Personal consultation with prof. Larissa Bravina, 12 September 2013.

[8] R. Stock, Landolt-Börnstein I 21A: Elementary particles 7 (2008), arXiv:0807.1610 [nucl-ex].

[9] L. Adamczyk *et al.* (STAR Collaboration), Phys. Rev. **D 86**, 072013 (2012).

[10] D. Tlustý for STAR Collaboration, Nucl. Phys. **A 904-905**, 639c (2013).

[11] J. Adams *et al.* (STAR Collaboration), Phys. Rev. Lett. **94**, 062301 (2005).

[12] M. Cacciari, P. Nason and R. Vogt, Phys. Rev. Lett. **95**, 122001 (2005).

[13] The STAR experiment at the Relativistic Heavy-Ion Collider, Brookhaven Natinal Laboratory; http://www.star.bnl.gov/

[14] M. Anderson, *et al.*; Nucl. Instrum. Meth. A **499** (2003) 659.

[15] W. J. Llope *et al.*, Nucl.Instrum.Meth. **A 522** (2004) 252-273.

[16] J. Beringer *et al.* (Particle Data Group), Phys. Rev. **D 86**, 010001 (2012).

[17] J. Crkovská (for STAR Collaboration), the European Physical Society Conference on High Energy Physics 2013, Proceedings of Science PoS(EPS-HEP 2013)037, http://pos.sissa.it/archive/conferences/180/037/EPS-HEP 202013_037.pdf.

Appendix A

Poster nad proceedings for the European Physical Society Conference on High Energy Physics 2013

Results of our analysis were presented as a poster at the EPS-HEP 2013 conference in Stockholm. Proceedings was accepted for publication at Proceedings of Science [17].

D^0 production in U+U collisions at $\sqrt{s_{NN}} = 193$ GeV at the STAR experiment

Jana Crkovská* for the STAR Collaboration
Faculty of Nuclear Sciences and Physical Engineering
Czech Technical University in Prague

Abstract

The relativistic heavy-ion collisions at RHIC in Brookhaven National Laboratory allow to produce a hot and dense nuclear matter - the Quark-Gluon Plasma (QGP). During the initial phase of the collision, enough energy is released from the hard scattering to produce the heavy quarks such as charm and bottom. The measurement of the production of mesons containing heavy quarks, such as D^0, in heavy ion collision is important to understand the properties of QGP. Due to their large mass, heavy quarks are expected to interact differently with QGP than light quarks.

The STAR experiment previously measured the production of charm mesons via hadronic channels in p+p, d+Au and Au+Au collisions. Charm quarks were observed to be strongly suppressed in Au+Au at high p_T. As U+U collision should produce even higher energy density, new information on heavy quark energy loss could be acquired. In this poster, the status of D^0 measurement in U+U collisions at $\sqrt{s_{NN}} = 193$ GeV via hadronic decay channel $D^0 \longrightarrow \pi^+ + K^-$ and $\overline{D^0} \longrightarrow \pi^- + K^+$ performed by STAR experiment is presented.

Previous D^0 Measurements at STAR

The D^0 meson: ($c\bar{u}$), $c\tau = 123$ μm, $m_D = 1.865$ GeV/c^2. STAR measured open charm mesons via hadronic decay $D^0 \longrightarrow \pi^+ + K^-$ and $\overline{D^0} \longrightarrow \pi^- + K^+$ with branching ratio BR = 3.89 %. Reconstruction of the hadronic mode enables a **direct identification**. However, the channel suffers from a **large combinatorial background** due to lack of precise secondary vertex measurement in STAR.
The STAR previously investigated $D^0 \longrightarrow \pi^+ + K^-$ and $\overline{D^0} \longrightarrow \pi^- + K^+$ channels in p+p ($\sqrt{s}$ = 200 and 500 GeV) [1,2], d+Au ($\sqrt{s_{NN}}$ = 200 GeV) [3] and Au+Au ($\sqrt{s_{NN}}$ = 200 GeV) [2] systems.

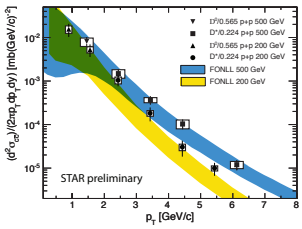

Left: The invariant differential charm cross-sections [2]. The data are compared to FONLL pQCD calculations [4]. The FONLL upper limit describes the data well.

Right: Nuclear modification factor (R_{AA}) in Au+Au 200 GeV [2]. The D^0 meson production is suppressed at high-p_T similarly as light hadrons.

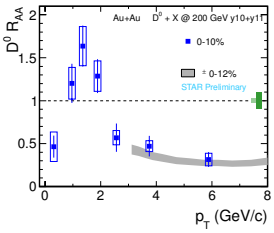

STAR detector

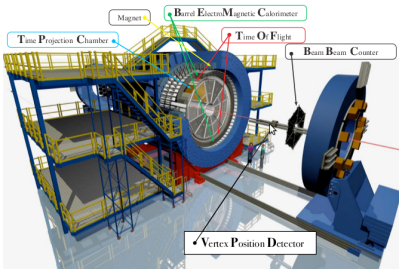

In current analysis, TPC and TOF subdetectors were used. Charged tracks were accepted from region:

$$-1 < \eta < 1 \qquad -\pi < \Delta\phi < \pi.$$

Data Analysis

Data: 320 millions of minimum-bias events collected in Year 2012 for U+U collisions at $\sqrt{s_{NN}} = 193$ GeV. D^0 and $\overline{D^0}$ reconstructed in $D^0 \longrightarrow \pi^+ + K^-$ and $\overline{D^0} \longrightarrow \pi^- + K^+$ channel, no secondary vertex information. Decay products were identified using a combination of TPC and TOF subsystems.

Only TPC: p_T range of 0.2 – 0.6 GeV/c and > 3.0 GeV/c.
- $n\sigma = (\ln dE/dx - \ln dE/dx_{meas})/R$
- $|n\sigma_K| < 2$ and $|n\sigma_\pi| < 2$

Only TOF: p_T range of 0.6 – 3.0 GeV/c.
- $1/\beta \in \left[\sqrt{\frac{m_\pi^2}{p^2}+1} - 2\sigma; \sqrt{\frac{m_K^2}{p^2}+1} + 2\sigma\right]$
- $\sigma_\pi = 0.0075$
- $\sigma_K(p) = 0.0076 + 0.0014/(1.89^{1.758p} - 1.152^{1.57})$

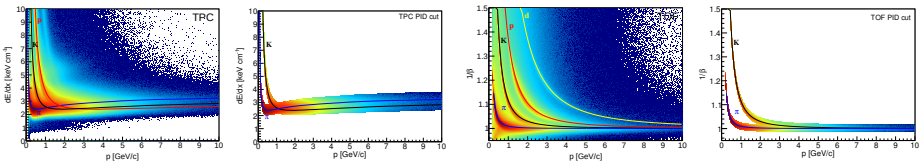

Double Counting

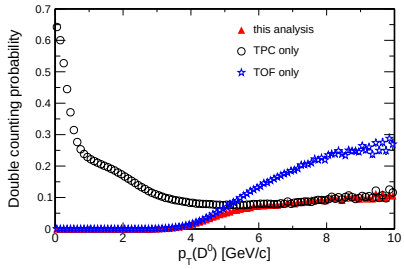

Kaons and pions may be misidentified as pions and kaons respectively. Such pairs then contribute to both D^0 and $\overline{D^0}$ count. Therefore we performed a **double counting** estimation for the analysis here presented.

- simple MC simulation using 500 M events
- misidentification probabilities determined from real data
- TPC gives high double counting in the lower p_T region, works well at $p_T > 3$ GeV/c
- TOF separates K from π very well at lower p_T, however it causes a greater double counting at $p_T > 3$ GeV/c

In the current analysis, the TPC was used at 0.2 – 0.6 GeV/c and > 3.0 GeV/c. The TOF covers the p_T window 0.6 – 3.0 GeV/c.

We were able to **correctly identify decay products up to p_T = 3 GeV/c**. At higher p_T, the double counting ratio **does not exceed 10%**.

Results

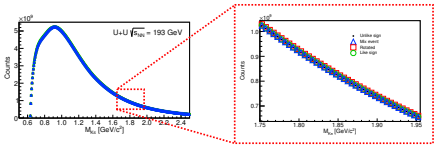

We have investigated the production of D^0 meson in the **transverse momentum range of 0.0 – 5.0 GeV/c**.
The **mixed-event method** has been used to describe the combinatorial background. This means that the daughter particles are selected from various different events. In this case, each kaon (pion) was combined with pions (kaons) from 5 different events.

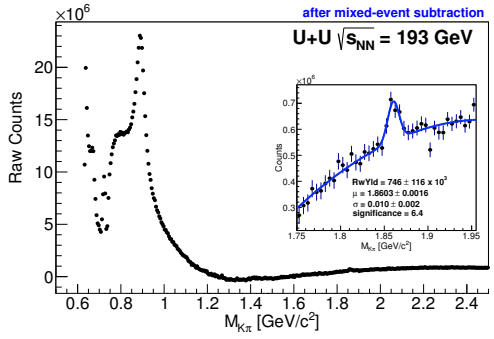

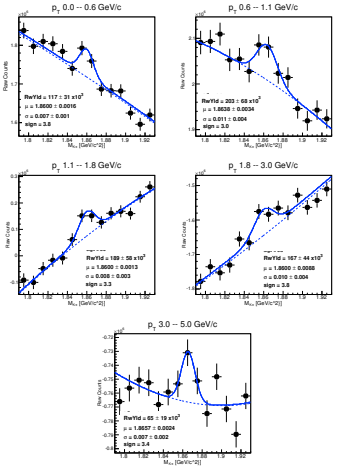

The signal was divided into **5 p_T bins**. The significance of signal in each bin was calculated as **significance** = $S/\sqrt{S+B}$
Possible improvements to increase signal significance are being investigated.

References

[1] L. Adamczyk *et al.* (STAR Collaboration), Phys. Rev. **D 86**, 072013 (2012).
[2] D. Tlustý for STAR Collaboration, Nucl. Phys. **A 904-905**, 639c (2013).
[3] J. Adams *et al.* (STAR Collaboration), Phys. Rev. Lett. **94**, 062301 (2005).
[4] M. Cacciari, P. Nason and R. Vogt, Phys. Rev. Lett. **95**, 122001 (2005).

Acknowledgement

This work was supported by the grant of the Grant Agency of Czech Republic n.13-20841S and by the Grant Agency of the Czech Technical University in Prague, grant No. SGS13/215/OHK4/3T/14.

*crkovjan@fjfi.cvut.cz. Presented at the 2013 European Physical Society Conference on High Energy Physics, Stockholm, Sweden, 18-24 July, 2013.

PROCEEDINGS OF SCIENCE

D^0 production in U+U collisions at $\sqrt{s_{NN}} = 193$ GeV at the STAR experiment

Jana Crkovská* **for STAR Collaboration**
Faculty of Nuclear Sciences and Physical Engineering, Czech Technical University in Prague, Břehová 7, Prague, Czech Republic
E-mail: crkovjan@fjfi.cvut.cz

The relativistic heavy-ion collisions at RHIC in Brookhaven National Laboratory allow to produce a hot and dense nuclear matter - the Quark-Gluon Plasma (QGP). During the initial phase of the collision, enough energy can be released from the hard scattering to produce heavy quarks such as charm and bottom. Due to their large masses, heavy quarks do interact differently with QGP than light quarks. The measurement of the production of mesons containing heavy quarks, such as D^0, in heavy ion collision is important to understand the properties of QGP.

The STAR experiment previously measured the production of charm mesons via hadronic channels in p+p, d+Au and Au+Au collisions. Heavy quarks were observed to be strongly suppressed in central Au+Au collisions. As U+U collision should produce even higher energy density, new information on heavy quark energy loss could be acquired. In this proceedings, the status of D^0 measurement in U+U collisions at $\sqrt{s_{NN}} = 193$ GeV via hadronic decay channel $D^0 \longrightarrow \pi^+ + K^-$ is presented.

The European Physical Society Conference on High Energy Physics -EPS-HEP2013
18-24 July 2013
Stockholm, Sweden

*Speaker.

1. Motivation

Open charm measurements are an important part of investigation of heavy-quark production in ultrarelativistic nuclear collisions. These measurements are important test of the pQCD calculations and also improve the understanding of the parton energy loss mechanisms in hot and dense nuclear matter. Previous measurements of nuclear modification factor of heavy quark particles indicate that there is similar suppression of charm and light hadrons at RHIC [1] although there is indication of some difference at LHC energies[2].

The hadronic decay $D^0 \longrightarrow K^- + \pi^+$ allows direct reconstruction of D^0 mesons. The drawbacks are large combinatorial background and a small branching ratio of 3.89%. Compared to previous STAR measurements of the hadronic channel $D^0 \longrightarrow \pi^+ + K^-$ [1,3,4], the U+U system is believed to provide new information on heavy quark energy loss.

2. Data Analysis

For the analysis presented here, minimum-bias events collected in Year 2012 for U+U collisions at $\sqrt{s_{NN}} = 193$ GeV were used. Decay products were identified using a combination of the Time Projection Chamber (TPC) and the Time of Flight (TOF) subsystems.

The TPC detector provides information about ionisation energy loss of the passing particle together with its momentum based on track curvature in magnetic field. TPC particle identification (PID) cuts were applied at $p_T = 0.2 - 0.6$ GeV/c and $p_T > 3.0$ GeV/c. Only tracks fulfilling $|n\sigma_K| < 2$ and $|n\sigma_\pi| < 2$ were accepted,where $n\sigma$ is a number of standard deviation from the expected value of ionisation loss $\mathrm{d}E/\mathrm{d}x$ for a given particle. The $n\sigma$ is defined as $n\sigma = (\ln \mathrm{d}E/\mathrm{d}x - \ln \mathrm{d}E/\mathrm{d}x_{meas})/R$, with R being the detector resolution. The TOF detector measures the velocity $1/\beta$ of the particles. Together with momentum information acquired from TPC, the mass of the particle can be calculated, providing a clear identification of the species. The TOF was used over p_T range of $0.6 - 3.0$ GeV/c. We required $1/\beta \in \left[\sqrt{\frac{m^2}{p^2}+1} - 2\sigma; \sqrt{\frac{m^2}{p^2}+1} + 2\sigma\right]$ where $\sigma_K = 0.0076 + 0.0014/(1.89^{1.758p} - 1.152^{1.57})$ and $\sigma_\pi = 0.0075$. The standard deviation was determined from the real data.

3. Results

We have investigated the production of D^0 meson for p_T up to 5.0 GeV/c. The mixed-event method has been used to describe the combinatorial background. Candidates for the daughter particles are selected from different events. In this case, each kaon (pion) was combined with pions (kaons) from 5 different events. The obtained mixed background was then normalised using a ratio of integral of unlike and mixed background over the invariant mass range $1.2 - 1.3$ GeV/c^2. The invariant mass distribution after background subtraction divided into 5 p_T-bins is shown in Fig. 1. The residual background was described using a second degree polynomial. The significance was calculated as $sign = S/\sqrt{S+B}$.

The preliminary results show that STAR can identify the $D^0 + \overline{D^0}$ signal in U+U collisions with significance larger or equal 3σ up to p_T of 5 GeV/c.

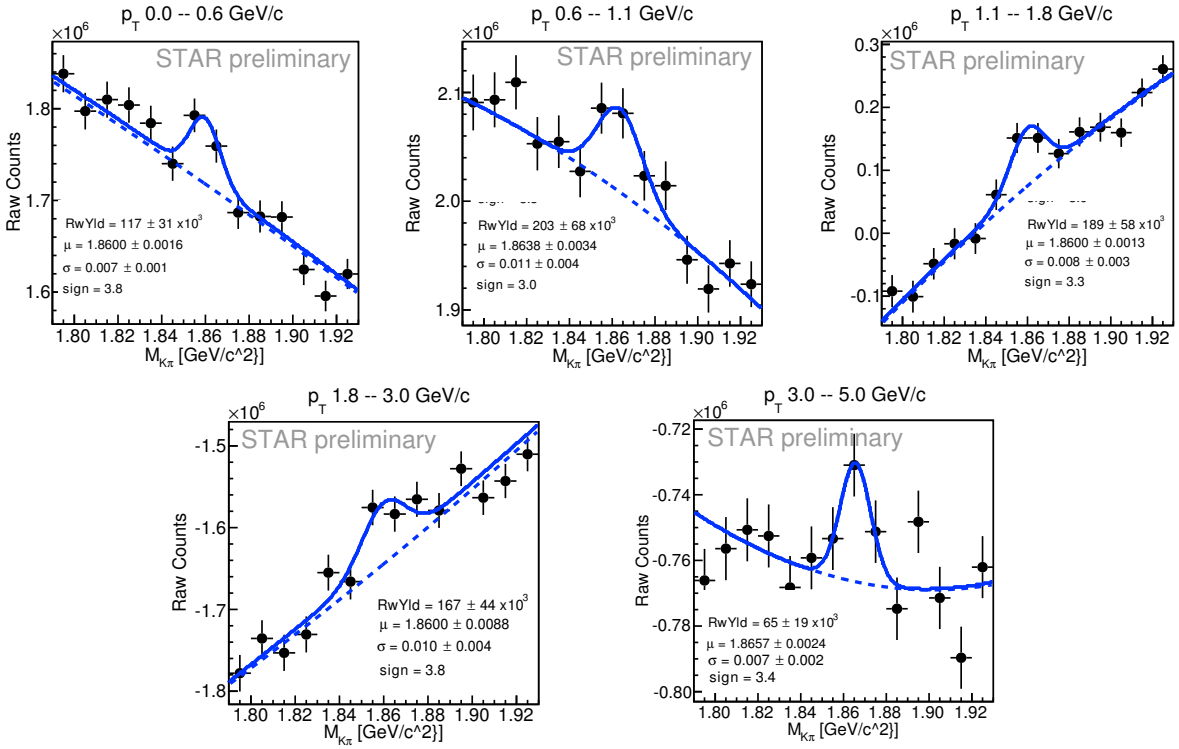

Figure 1: Invariant mass distribution for $K^{\pm}\pi^{\mp}$ pairs in U+U at $\sqrt{s_{NN}} = 193$ GeV after mixed-event background subtraction.

Acknowledgement

This work was supported by the grant of the Grant Agency of Czech Republic n.13-20841S and by the Grant Agency of the Czech Technical University in Prague, grant No. SGS13/215/OHK4/3T/14.

References

[1] D. Tlustý *et al.* (STAR Collaboration), Nucl. Phys. **A 904-905**, 639c (2013).

[2] B. Abelev *et al.* (ALICE Collaboration), JHEP 09 (2012) 112.

[3] L. Adamczyk *et al.* (STAR Collaboration), Phys. Rev. **D 86**, 072013 (2012).

[4] J. Adams *et al.* (STAR Collaboration), Phys. Rev. Lett. **94**, 062301 (2005).

[5] M. Cacciari, P. Nason and R. Vogt, Phys. Rev. Lett. **95**, 122001 (2005).